J. Min. Metall. Sect. B-Metall., 56 (2) B (2020) 171 - 182

Journal of Mining and Metallurgy, Section B: Metallurgy

EFFECT OF CARBON AND MANGANESE CONTENT ON THE MICROSTRUCTURE AND MECHANICAL PROPERTIES OF HIGH MANGANESE AUSTENITIC STEEL

U. Gürol [a*] and S. Can Kurnaz [a]

[a] Sakarya University, Engineering Faculty, Department of Metallurgical & Materials Engineering, Sakarya, Turkey

(Received 11 November 2019; accepted 11 February 2020)

Abstract

In the present work, the influence of carbon and manganese on the microstructure and the mechanical properties of high manganese austenitic steel were investigated. Increased carbon and manganese content increased the grain size and the amount of carbides in the as-cast condition. The solution annealing fully dissolved the carbides in the alloys with lower carbon content (1wt%) and resulted in a homogeneous austenitic microstructure. The yield strength, ultimate strength, Charpy, and elongation were increased by the combination of carbon and manganese. Optimal results were obtained in the solution annealed 1.0C-17Mn alloy, respectively, 415.0±4.1MPa 865.6±1.5 MPa, 65.2±0.8%, and 258±3 J. The wear tests were performed under the loads of 2.5N, 5N, 10N and 15N with a ball-on-disc wear testing machine at constant speed of 0.2 ms^{-1} for sliding distance of 500m; it was revealed that 1C-21Mn alloy could be applied to relatively high-stress wear conditions while the 1.3C-17Mn alloy could be only used under low-stress wear conditions.

Keywords: *Hadfield steel; Microstructure characterization; Tensile properties; Charpy-V-notch; Wear resistance*

1. Introduction

Hadfield manganese steel was invented by Sir Robert Hadfield in 1882 and first patented in Britain in 1883 with patent number 200 [1], and consequently, in 1884 the patents 303150 and 303151 were granted in the United States [2]. Most of the steels which were used prior to the invention of Hadfield steel were of much lower alloy content, showing an inverse relationship between hardness and toughness [3]. Hence, the invention of these alloys was based on adding a large percentage of manganese to the molten iron which yields a steel product with an outstanding combination of strength, ductility, and strain hardening compared to the early ones [4,5]. The basic chemical composition of Hadfield steel includes 1.0-1.4 wt% carbon and 10-14 wt% manganese in a 1:10 ratio [6]. This steel, with small changes in its chemical composition or heat treatment, is widely used in various fields of industry such as mining, earthmoving, quarrying, oil-well drilling, steel-making, cement clay products, rail-roading, dredging, naval, lumbering excavators, and crushers [6-8].

It is well known that a high manganese austenitic steel is too brittle in the as-cast condition due to the precipitation of carbides in the grain boundaries which limits its applications in the fields requiring high ductility and toughness [9,10]. Hence, these steels have to be heat treated above the A_{cm-} line of the phase diagram, the procedure referred to as solution annealing, followed by rapid water quenching [11]. This process dissolves the carbides precipitated as a result of eutectic transformation of the liquid-rich in carbide forming elements at the end of solidification, and ensures a fully austenitic microstructure with a face-centered cubic crystal lattice with interstitial carbon and manganese atoms [12,13]. The solution temperature should be chosen to be more than 1000°C followed by water quenching in order to dissolve carbides into the austenite matrix [9], but not more than 1100°C to avoid carbon segregation that may cause incipient melting, scaling, and decarburization [14].

There are two significant stages during producing desirable parts from high manganese steels: first melting and developing of appropriate composition, and than proper heat treatment of the cast parts [15]. In this context, a wide range of research has been carried out for improving the mechanical properties of the high manganese steels for long service. These

**Corresponding author: ugur.gurol@yahoo.com*

https://doi.org/10.2298/JMMB191111009G

include the addition of chromium [16], molybdenum [1], vanadium [17], niobium [18], titanium [19], aluminum [20], and cerium [11] in combination with heat treatment. Moreover, the mechanical properties of high manganese steels are very dependent on carbon and manganese contents [21]. These two elements play an essential role in promoting precipitation strengthening and therefore strongly influence the mechanical properties such as tensile properties, impact toughness, and wear resistance [22]. Lu Dingshan et al. [23] studied the influence of carbon content on the microstructure and mechanical properties of Mn13Cr2 and Mn18Cr2 steel. They reported that the proportions of carbide in these two steels increased with increased carbon content, while the impact toughness of the as-cast and water quenched Mn13Cr2 and Mn18Cr2 steels decreased. However, this research was carried out in a small scope of carbon concentration range (1.25 wt% -1.45 wt%), and hence it did not show the effect of lower carbon amount on mechanical properties. Torabi et al. [24] investigated the effect of manganese content (7.55 wt%, 13.1 wt%, and 16.5 wt%) on the properties of high manganese austenitic steels and concluded that with increasing manganese from 7.55 wt% to %16.5 wt%, the ultimate tensile strength and wear resistance showed 11% and 29% increases, respectively, due to solid solution strengthening of the matrix with manganese. In their study, the manganese content was limited to 16.5 wt%.

However, no extensive research has been reported for the effect of simultaneous addition of carbon and manganese to optimize the microstructure and mechanical properties of high manganese austenitic steels. Optimization of ultimate tensile, impact toughness, and wear resistance of the high manganese steel is a key factor to increase the service life of critical engineering components. The current aimed to produce a high-performance manganese steel with a fully austenitic microstructure without carbide precipitation and to obtain excellent mechanical properties in terms of wear resistance without sacrificing the toughness and tensile properties by adjusting the manganese content (13 wt%, 17 wt%, and 21 wt%) and carbon percentages (07 wt%, 1.0 wt%, and 1.3 wt%). The specific adjustment of the manganese and carbon content can reduce the premature failures and part replacement of such steels in the industry.

2. Materials and methods

The alloys were obtained by adjusting the chemical composition in conventional melting using classified steel scraps and standard silicon, manganese, and molybdenum ferroalloys. An industrial-scale induction furnace with a maximum capacity of 3000 kg was used to heat raw materials up to 1480°C. When the raw material was fully melted, the proper amount of ferroalloys were added and left in the furnace for 15 minutes to homogenize and to achieve required alloy compositions. Then, molten steel was transferred to the ladle at 1480°C and chemical analysis was performed by the ARL optical emission spectrometer according to the ASTM E2209 standard from chilled samples taken from the inside of the transferred ladle. Finally, ten test coupons with dimensions of 60x60x300 mm^3 were cast into a chromite sand mold at the pouring temperatures of 1440°C and 1450°C. The identification and composition of alloys are given in Table 1.

Table 1. *Chemical composition of alloys (wt%)*

Alloy	C	Mn	Si	Mo	P, S	Fe
0.7C-17Mn	0.70	17.13	0.56	1.18	<0.05	Balance
1.0C-13Mn	1.00	13.11	0.53	1.15	<0.05	Balance
1.0C-17Mn	1.00	17.11	0.53	1.16	<0.05	Balance
1.0C-21Mn	1.03	20.79	0.56	1.18	<0.05	Balance
1.3C-17Mn	1.27	17.02	0.51	1.16	<0.05	Balance

A heat treatment process which included heating the specimens to 650°C and holding at this temperature for 3 hours was performed with an oxygen-controlled custom-built automatic heat treatment furnace (Sistem Teknik Industrial Furnaces). This mid-process reduced the amount of pearlite in the as-cast condition and prevented internal crack formation during heating. This was because as the pearlite transformed, the austenization rate accelerated and contributed to increased carbon dissolution into the austenite matrix. After holding specimens were heated to 1100°C at the rate of 1.67°C/min and subjected to solution annealing for 3 hours and then quenched in 90 tonnes of the circulated water tank at 27°C. The heat treatment process is shown in Fig 1.

Metallographic examination was performed according to ASTM E3-11 (metallographic sample preparation) and ASTM E407-07 (metal micro-

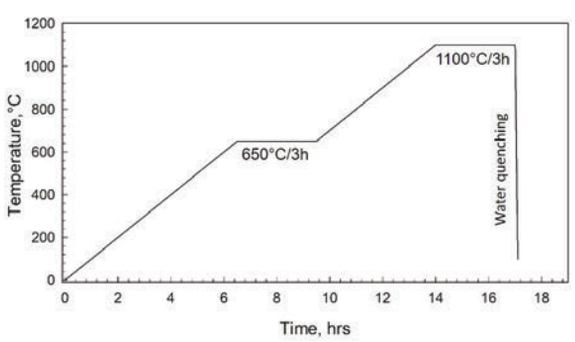

Figure 1. *Heat treatment process of the alloys*

etching) standards. The sectioned specimens for metallography were ground, polished, and etched with 4 wt% Nital solution for 10s. The microstructures of the as-cast and solution annealed specimens were characterized using an optical microscope (OM, Olympus PME Tokyo) and a scanning electron microscope (SEM, FEI Quanta FEG 450) equipped with energy disperse spectrometry (EDS, EDAX Octane Plus). The fracture surface of the Charpy-V-notch samples was further analyzed by means of SEM. In addition, X-Ray diffraction spectrometry (XRD, Rigaku DMax 2200) using CoKα radiation was performed to analyze the phases and precipitates of the alloys. The average grain size of each alloy was measured utilizing the intercept method according to the ASTM standard E112-13 (standard test methods for determining average grain size) by using the Image-J software (version 1.51k) which was also used to determine the carbide volume fraction of the alloys. The solidus and liquidus temperatures were calculated using the JMatPro simulation software for the alloys as predicted by the thermodynamic calculation.

The surface hardness of the samples was measured using a Brinell hardness tester at an applied load of 30 kgf and loading times of 20 seconds at room temperature in compliance with ASTM E10-18 standard. Tensile testing was performed with an Instron test machine, model 300LX employing an average of three specimens for each sample with the respect to ASTM E8/E8M. The impact test of the samples was carried on 10x10x55 mm^3 at room temperature, using a 300J capacity test machine, with the Charpy V-notch test method according to ASTM E23. The ball-on-disc wear test was carried out in accordance with ASTM G99-05 standard. The tests were performed at room temperature with a 10 mm diameter alumina ball as the counter body. The weight loss of each sample was measured under 2.5 N, 5 N, 10 N, and 15 N normal loads at 0.2 ms^{-1} sliding speed with 500 m sliding distance without stopping the tests.

3. Results and discussion

3.1. Characterization of the as-cast structures

Fig. 2a-e illustrates the effect of carbon and manganese content on the as-cast microstructure of the alloys by an OM. The 0.7C-17Mn alloy had an austenite matrix with a small fraction of carbide while other as-cast alloys showed the austenite matrix surrounded by a dispersed lamellar carbide. The presence of austenite was due to the high level of carbon and manganese, and carbide was due to the presence of high carbon and carbide forming elements such as manganese, molybdenum, and iron. The carbides formed during slow cooling which started near grain boundaries and proceeded into the former grains.

XRD results of as-cast alloys in Fig.2f indicated that austenite (γ) was the major phase with $(FeMn)_3C$ carbide precipitation which is consistent with the micrographs in Fig. 2a-e. The volume fractions of the carbides for as-cast alloys generated within the grains and at the boundaries were obtained by Image-J software and presented in Table 2. Increased carbon content from 1.0 wt% to 1.3 wt% for the same level of manganese content (17 wt%) significantly increased the amount of carbides from 6.1±2.5 % to 23.9±2.3%. Similarly, as the manganese content increased from 13 wt% to 21 wt%, the carbide content increased from 7.5±1.7 % to 18.6±2.6 %, approximately 2.5 times. This can be explained by the fact that the addition of Mn or C increases the carbide solvus temperature and therefore carbide solubility decreases.

The austenite grain size of the produced alloys was measured by the linear intercept method by counting the grain boundaries and the results are

Table 2. *Volume fraction of carbides and austenite in as-cast alloys (%)*

	0.7C-17Mn	1.0C-13Mn	1.0C-17Mn	1.0C-21Mn	1.3C-17Mn
Carbides	<1	7.5 ± 1.7	6.1 ± 2.5	18.6 ± 2.6	23.9 ± 2.3
Austenite	Balance	Balance	Balance	Balance	Balance

Table 3. *Grain size of alloys in as-cast and solution annealed condition*

	0.7C-17Mn	1.0C-13Mn	1.0C-17Mn	1.0C-21Mn	1.3C-17Mn
As-Cast Steels	197 ± 3 μm	172 ± 11 μm	243 ± 20 μm	412 ± 29 μm	427 ± 24 μm
Solution Annealed	281 ± 18 μm	215 ± 10 μm	338 ± 26 μm	619 ± 27 μm	589 ± 38 μm

Table 4. *Comparison of liquidus and soludius temperature of alloys (with Jmat-Pro Software)*

(°C)	0.7C-17Mn	1.0C-13Mn	1.0C-17Mn	1.0C-21Mn	1.3C-17Mn
Liqudus Temp.	1405	1395	1380	1365	1360
Solidus Temp.	1305	1270	1255	1240	1205
Freezing Range	100	125	125	125	155

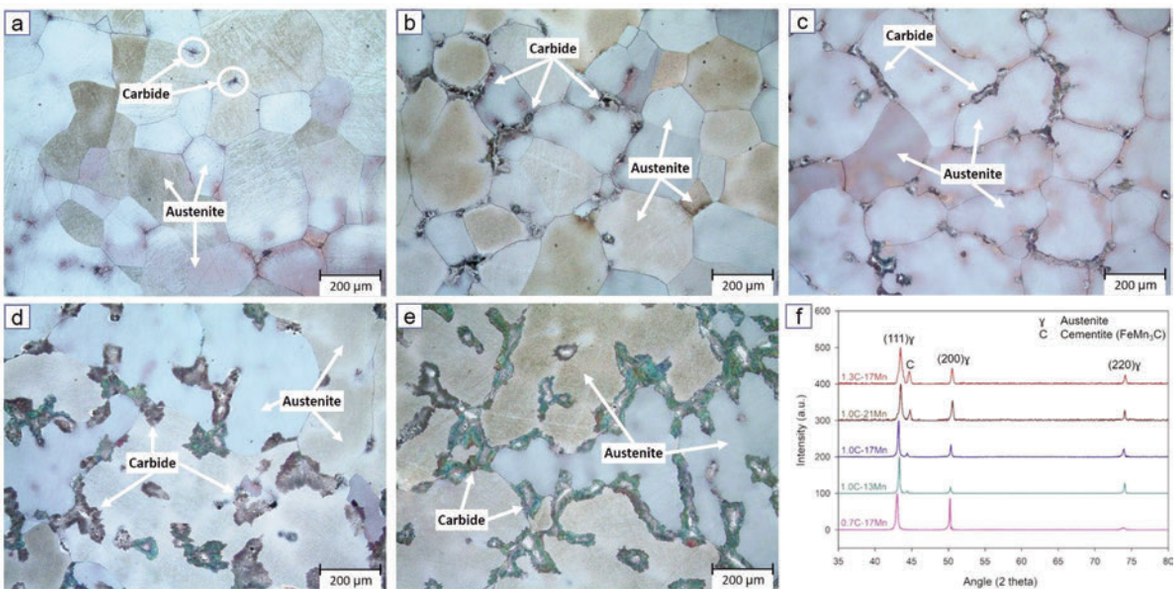

Figure 2. *Optical micrographs showing the as-cast microstructure of alloys: (a) 0.7C-17Mn, (b) 1.0C-13Mn, (c) 1.0C-17Mn, (d) 1.0C-21Mn, (e) 1.3C-17Mn and (f) XRD patterns of the as-cast alloys*

shown in Table 3. The grain size of as-cast alloys ranged from 172±11 µm to 427±24 µm. Increased carbon and manganese content led to grain coarsening which had a direct influence on the mechanical properties. Increasing the carbon content extended the freezing range and consequently led to longer solidification, which may have caused the larger grain size. As an example, as shown in Table 4, increasing the carbon content from 0.7 wt% to 1.3 wt% decreased the liquidus and solidus temperatures by an average of 45°C and 100°C, respectively. This resulted in the freezing range of 1.3C-17Mn alloy to increase ~1.5 times compared to 0.7C-17Mn alloy. Consequently, the grain size of 1.3C-17Mn alloy was two times larger than 0.7C-17Mn alloy. Moreover, liquidus and solidus temperature decreased by 5°C with the addition of per 1 wt% manganese, although this did not change the freezing range. In this case, the reason for the larger grains with increased manganese can be explained that the manganese is conducive to the growth of coarse grains [23].

The detailed microstructural characteristics of the secondary precipitates were revealed in Fig. 3 by means of SEM. Such observations showed that 0.7C-17Mn alloy had a very thin grain boundary carbides while the 1.0C-17Mn and 1.3C-17Mn alloys had two-phase lamellar carbides along the grain boundaries. Energy dispersive spectroscopy (EDS) was used to determine the composition of secondary precipitates and two distinct carbides were revealed: $(Fe,Mn)_3C$ and MoC [25]. Molybdenum carbides, which were not found in XRD due to their small volume fraction in the microstructures, were mainly distributed in the grain boundaries and surrounded by lamellar carbides. Since molybdenum has a high affinity to absorb carbon [26], first there were more stable molybdenum carbides instead of iron manganese carbide at the grain boundaries. Furthermore, the ternary phosphorus eutectic of a Fe-$(Fe,Mn)_3C$-$(Fe,Mn)_3P$ type was found in the center of lamellar carbides as previously reported with ASTM A128/A128M Gr. B3 manganese steel (1.2 wt% C, 13 wt% Mn and 0.027 wt% P) [27], which can also be seen in the microstructures in ASM Handbook Vol.9, where the mottled area in the centers of lamellar carbides was identified as phosphide eutectic [28]. This ternary eutectic was mostly blocky and not elongated along the grain boundaries (point 2 in both Fig.3b and 3c). However, when the castings are heated at the correct solution temperature, this ternary eutectic re-dissolves into the austenitic matrix and loses its harmful effect [29].

3.2. Characterization of solution annealed structures

Fig. 4 shows the microstructures of the alloys after solution annealing at 1100°C for 3 hours. The SEM micrograph of the 1.0C-17Mn sample showed a fully austenitic microstructure which indicates that the designed solution annealing and subsequent rapid quenching had been successful in dissolving all the precipitates into the matrix (Fig. 5a). However, the grain size of the alloys had increased. Moreover, the 1.3C-17Mn alloy had grain boundary carbides and phosphide eutectic as shown in Fig. 5b. Compared to the 1.0C-17Mn sample, the higher level of carbon in the 1.3C-17Mn alloy required higher temperatures or longer times for the dissolution of the carbides and phosphide eutectic. However, the high manganese

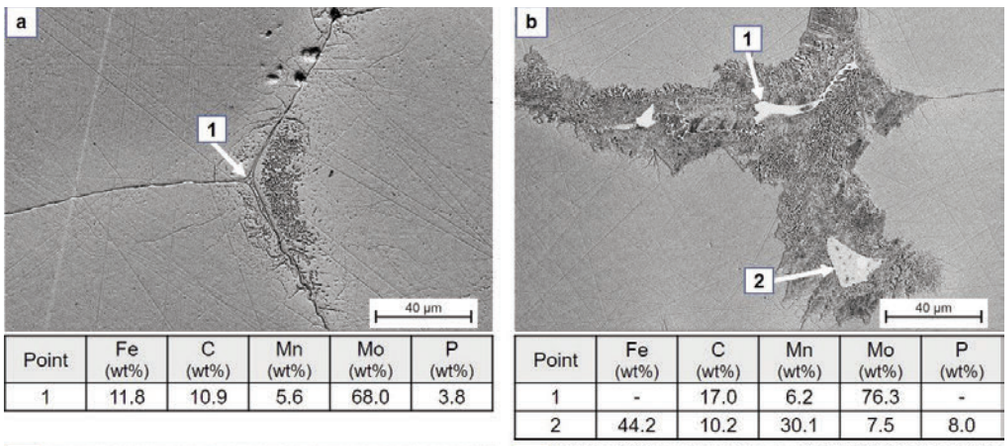

Point	Fe (wt%)	C (wt%)	Mn (wt%)	Mo (wt%)	P (wt%)
1	11.8	10.9	5.6	68.0	3.8

Point	Fe (wt%)	C (wt%)	Mn (wt%)	Mo (wt%)	P (wt%)
1	-	17.0	6.2	76.3	-
2	44.2	10.2	30.1	7.5	8.0

Point	Fe (wt%)	C (wt%)	Mn (wt%)	Mo (wt%)	P (wt%)
1	-	12.7	10.3	77.0	-
2	46.3	9.7	31.5	4.9	7.6
3	57.3	10.2	29.8	2.6	-

Point	Fe (wt%)	C (wt%)	Mn (wt%)	Mo (wt%)	P (wt%)
1	57.3	11.9	25.8	4.7	0.3

Figure 3. *SEM micrograph (BSE mode) and EDS results of alloys in as-cast condition: (a) 0.7C-17Mn (b) 1.0C-17Mn, (c) 1.3C-17Mn, (d) 1.3C-17Mn showing the detailed two-phase lamellar carbide precipitation*

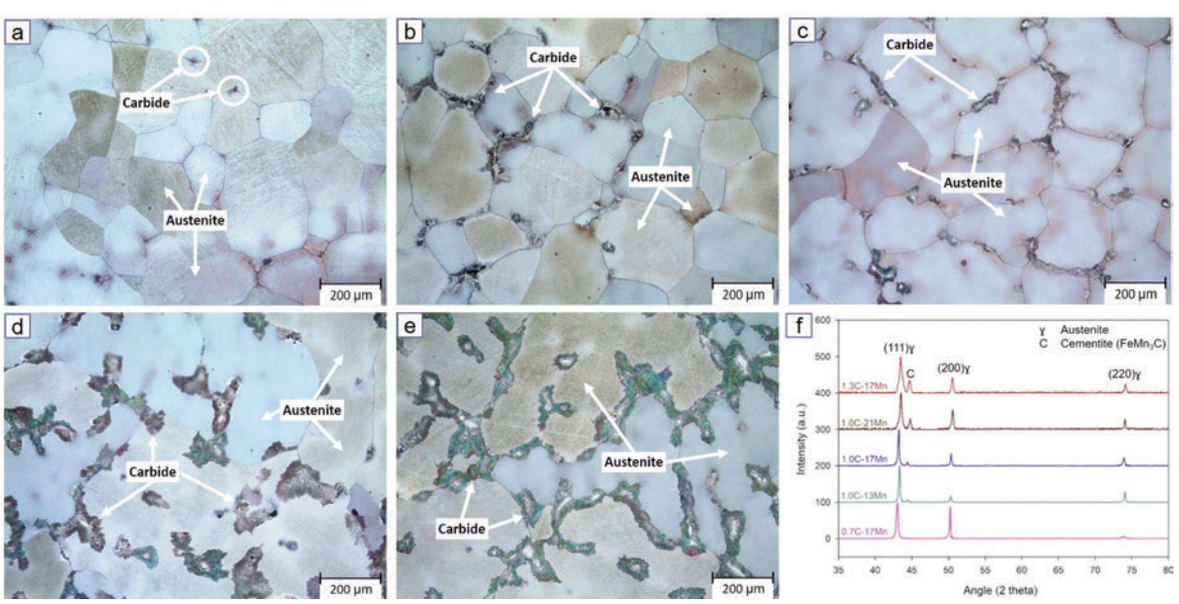

Figure 4. *Optical micrographs showing the solution annealed microstructure of alloys: (a) 0.7C-17Mn, (b) 1.0C-13Mn, (c) 1.0C-17Mn, (d) 1.0C-21Mn, (e) 1.3C-17Mn and (f) XRD patterns of the alloys after solution annealing*

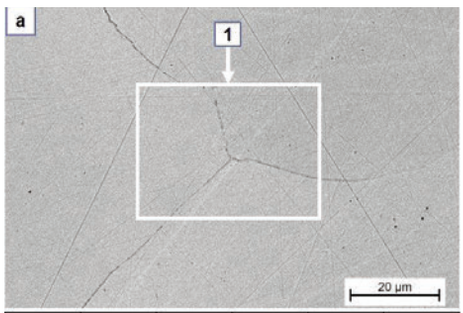

Point	Fe (wt%)	C (wt%)	Mn (wt%)	Mo (wt%)	P (wt%)
1	76.1	4.1	18.0	1.45	-

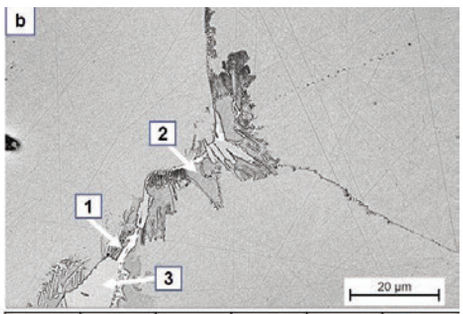

Point	Fe (wt%)	C (wt%)	Mn (wt%)	Mo (wt%)	P (wt%)
1	-	11.8	8.7	79.5	-
2	52.9	9.5	34.4	3.1	-
3	50.8	7.7	27.0	6.5	8.0

Figure 5. *SEM micrographs (BSE mode) of alloys in solution annealed condition: (a) 1.0C-17Mn and (b) 1.3C-17Mn*

steels suffer from a sharp decline of the mechanical properties at high temperatures, and therefore temperatures above 1100°C should be avoided [14].

3.3. Mechanical Properties

Hardness measurements before and after solution annealing are given in comparison with carbide contents in Fig.6. Increased carbon and manganese increased the hardness of all as-cast alloys. For example, the hardness of the as-cast 1.3C-17Mn alloy was almost 27% higher than the as-cast 0.7C-17Mn alloy due to the existence of 23.9±2.3% volume fraction of carbides. A similar trend was observed for the increase of the hardness with carbon for the solution annealed samples. The underlying strengthening mechanism was the carbide precipitation and solid solution strengthening of the matrix by these elements. Moreover, the solution annealed samples showed higher hardness values compared to their cast states, except for the 1.3C-17Mn and 1.0C-21Mn alloys. The increase in hardness can be attributed to the fairly uniform distribution of the carbide phase in the austenite phase

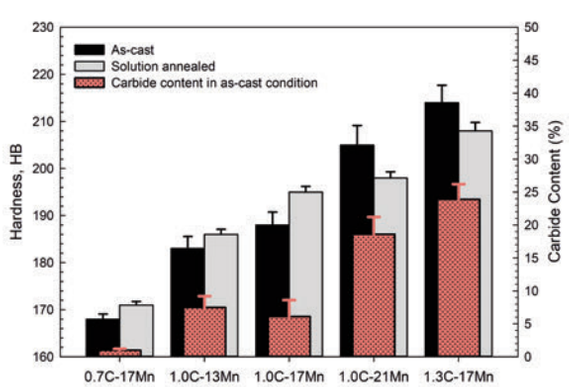

Figure 6. *Hardness test results of alloys in as-cast and solution annealed condition in comparison with as-cast carbide content*

[5]. The decrease in the hardness of the solution annealed 1.3C-17Mn and 1.0C-21Mn alloys compared to the cast ones can also be explained by heterogeneous carbide distribution. Hence, for these two alloys, a high amount of grain boundary carbides in the as-cast structure acted as a hard phase in the soft austenite matrix and increased overall hardness value.

The room temperature tensile test results of the alloys before and after solution annealing, including the yield strength ($Rp_{0.2}$), ultimate strength (Rm), and elongation (%) are listed in Table 5. Increasing the carbon and manganese content caused an increase in the yield strength despite grain coarsening which is in opposition to the Hall-Petch effect [30]. The strengthening effect can be due to the solid solution strengthening as previously reported [23-24].

Fig. 7a shows that, except for the 0.7C-17Mn alloy, the engineering stress-strain curves of as-cast alloys were quite different from their solution annealed conditions. The presence of carbide and phosphorus eutectic in the as-cast states led to steep strain hardening during the plastic regime, followed with an abrupt rupture and a very low macroscopic deformation. Accordingly, the highest ultimate tensile and elongation, 804.6±13.9 MPa and 60.8±3.4 %, respectively, were obtained with 0.7C-17Mn sample which had thin grain boundary carbides observed at high magnification by SEM (see Fig.3a). Thin carbides are less stable and have a good lattice match and cohesion with the austenite matrix because of their small size and low energy [29]. As shown in Fig. 7b, solution annealed alloys showed a continuous yielding behavior followed by considerable strain hardening. Compared to the as-cast ones, they also showed increased ultimate tensile and elongation. All the solution annealed alloys showed excellent plastic deformation, above 40%. Fig. 4 compared to Fig. 2 showed that this was due to carbide re-solution into the austenite matrix. In other words, the reduced carbide content at the grain boundaries increased the deformability of the samples.

Table 5. *Room temperature tensile test results of alloys in as-cast and solution annealed conditions*

Alloys	Process	Rp0.2 (MPa)	Rm (MPa)	Elongation (%)
0.7C-17Mn	As-cast	349.6 ± 2.2	804.6 ± 13.9	60.8 ± 3.4
	Solution annealed	369.9 ± 4.4	852.7 ± 5.4	77.4 ± 2.5
1.0C-13Mn	As-cast	374.1 ± 4.3	516.9 ± 3.3	10,3 ± 0.1
	Solution annealed	395.4 ± 5.2	827.3 ± 2.8	54.6 ± 0.3
1.0C-17Mn	As-cast	398.1 ± 2.4	601.6 ± 2.9	17.3 ± 0.4
	Solution annealed	415.0 ± 4.1	865.6 ± 1.5	65.2 ± 0.8
1.0C-21Mn	As-cast	408.1 ± 5.2	500.7 ± 16.3	7.0 ± 0.5
	Solution annealed	411.3 ± 6.3	728.9 ± 11.6	47.9 ± 1.5
1.3C-17Mn	As-cast	421.6 ± 3.0	537.1 ± 1.4	4.4 ± 0.3
	Solution annealed	437.1 ± 7.1	743.8 ± 28.1	40.6 ± 3.6

The 1.0C-17Mn alloy showed the highest tensile strength (865.6±1.5 MPa) and elongation (65.2±3.4%). By increasing carbon up to 1.3 wt% with the same manganese content (17 wt%), it was increasingly difficult to dissolve all of the carbon in solid solution, hence elongation and ultimate tensile slightly decreased. On the other hand, by increasing the manganese content from 13 wt% to 17 wt% Mn, the stacking fault energy was increased and therefore the shear stress needed for sliding increased [31]. This has led to increased ultimate tensile and elongation. However, at 21 wt% Mn, the austenite grain size sharply increased from 338±26μm to 619±27μm, almost two times. This resulted in the ultimate tensile and elongation decreasing compared to 1.0C-17Mn. Since the grain boundaries help to prevent further dislocation propagation, smaller grain sizes led to higher yield and tensile strength [9,30].

Fig. 8 shows optical micrographs of solution annealed alloys 1.0C-17Mn and 1.3C-17Mn after tensile testing. The main deformation mechanism was assumed to be twinning induced deformation in both alloys. The twin boundaries act as strong barriers to dislocation motion which leads to work hardening and an increase of elongation and ultimate tensile strength [32-33]. There were fewer twins in the 1.3C-17Mn alloy compared to the 1.0C-17Mn alloy. This was due to the presence of undissolved carbides along the grain boundaries of the 1.3C-17Mn alloy (arrows in Fig. 8b). Black areas in both Fig.8a and Fig.8b show the cavities left behind by dissolved phosphide eutectic [29]. With increased carbon content, twinning energy weakened and carbides along the grain boundaries caused crack initiation and grain detachment by crack growth occurred during the tensile testing and hereby resulted in low elongation and tensile strength.

Toughness is another main characteristic feature of high manganese steel under severe load conditions [34], which should be considered as one of the important factors in the optimization of these cast steels. It is already known that most metals, especially with FCC structure such as high manganese steels have a ductile fracture at ambient temperature. The brittle fracture for high manganese steels can be attributed to the existence of continuous carbide networks at grain boundaries [35].

Fig. 9 shows the Charpy impact test results of alloys in as-cast and solution annealed conditions. The impact toughness of the as-cast alloys, except 0.7C-

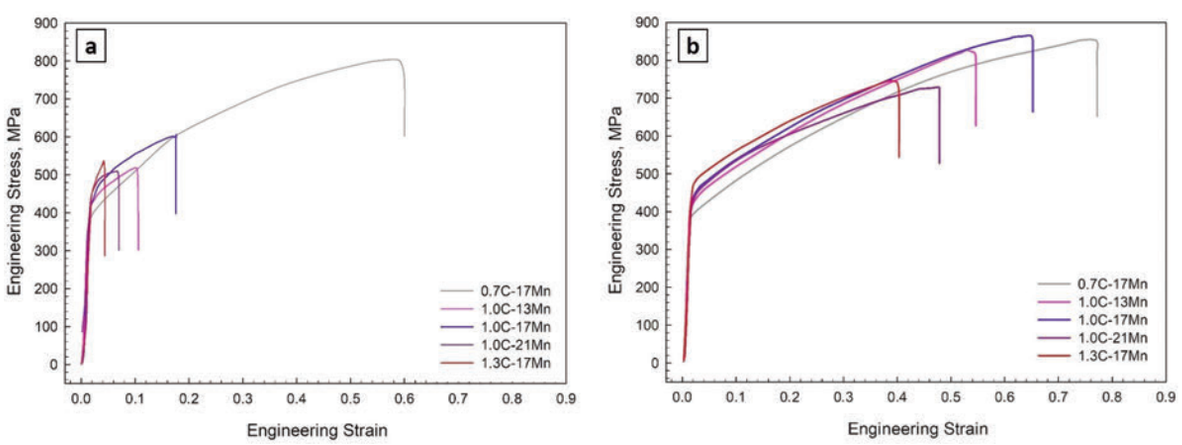

Figure 7. *Engineering stress-strain curves: (a) as-cast and (b) solution annealed alloys*

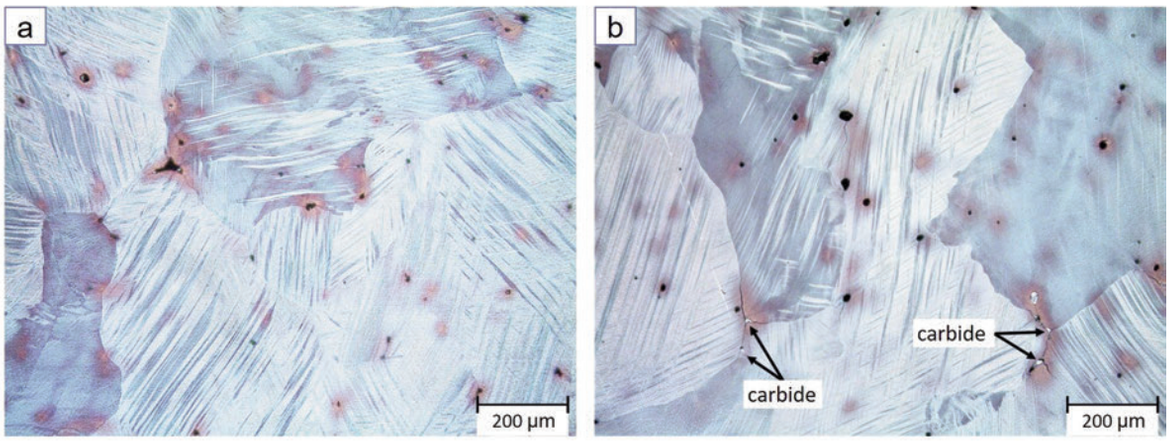

Figure 8. *Optical micrographs of solution annealed alloys after fracture in the tensile test: (a) 1.0C-17Mn and (b) 1.3C-17Mn*

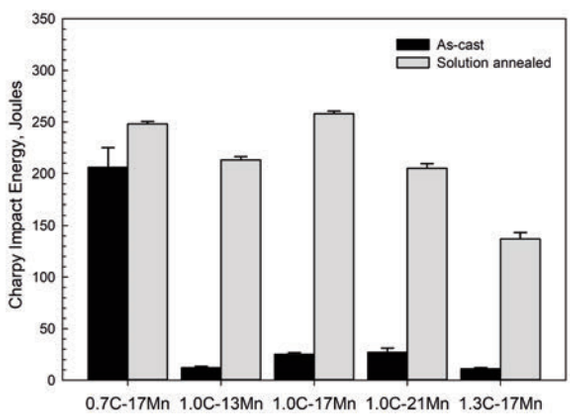

Figure 9. *Charpy impact test results of alloys in as-cast and solution annealed conditions*

17Mn, was about 12 to 27 Joules at room temperature, which seems to be insufficient for most of the engineering applications such as crusher jaws where the impact load is applied [36]. Since the brittle carbides, segregated along the austenite grain boundaries which cause stress built-up in the austenite matrix, leading to dislocation pile-up, crack initiation, propagation and crack growth and subsequently low impact toughness in as-cast condition [37]. Only as-cast 0.7C-17Mn alloy which showed very thin grain boundary carbides, showed a high impact toughness value reaching up to 206±19 Joules which allows for the mining and earthmoving applications.

It is already seen that the solution annealing considerably increased the impact toughness of the alloys compared to the as-cast ones. The largest improvement was for the 1C-17Mn alloy with an almost ~930% increase in toughness. The reason for such a high value was complete austenization of structure and absence of carbide re-precipitation along the grain boundaries. The lowest impact energy in the solution annealed samples was for the 1.3C-17Mn alloy at 137±6 Joules because of the undissolved carbides and phosphide eutectic along the grain boundaries.

Fig. 10a shows the fraction surface of 1.0C-17Mn alloy after the Charpy impact test, revealing a typical ductile fracture model. A large number of dimples existed in the fracture surface. Since the 1.3C-17Mn

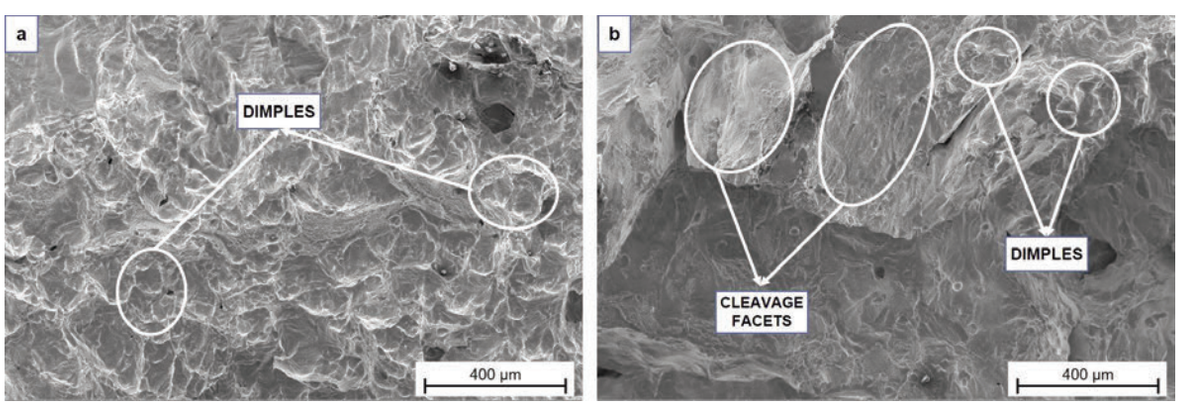

Figure 10. *SEM micrograph (SE mode) of Charpy V-notch impact samples of alloys in solution annealed condition (a) 1.0C-17Mn and (b) 1.3C-17Mn*

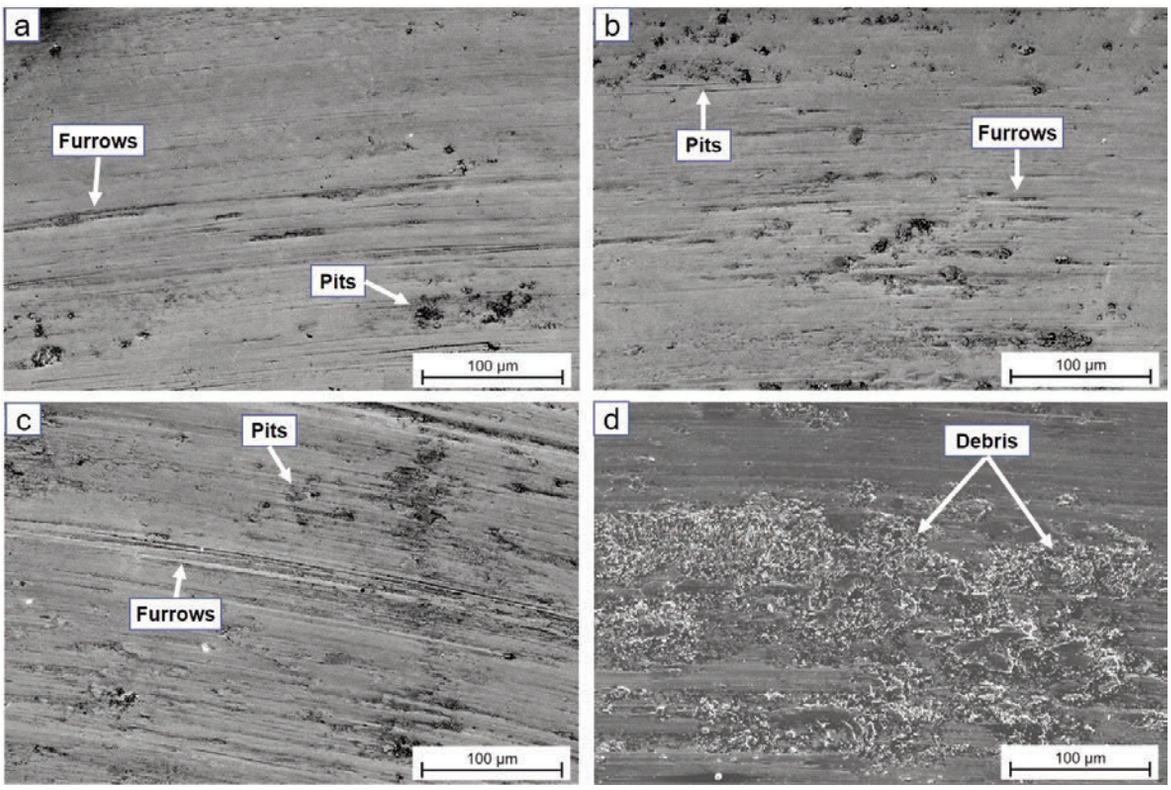

Figure 11. *SEM micrograph (SE mode) of worn surface for solution annealed 1.0C-17Mn alloy under normal loads of : (a) 2.5 N, (b) 5 N, (c) 10 N and (d) 15 N*

alloy showed a mixture of ductile and brittle fracture with a characteristic of dimples and quasi-cleavage facets (Fig.10b). Increased carbon content resulted in a serious decrease in dimples and increased cleavage facets which accelerated crack propagation and decreased the impact energy [38]. The reason for the simultaneous activation of ductile and brittle fracture mechanism was due to the presence of undissolved carbides in the austenite grain boundaries as shown previously in Fig.5b. In high manganese steels the most important parameter for controlling the fracture mode is the volume fraction of carbides along the grain boundaries [35]. By increasing the volume fraction of carbide in austenite matrix, the crack growth in austenite grain boundaries reaches the critical value before the shear stress causes plastic deformation of the austenite phase, resulting in a brittle fracture [35].

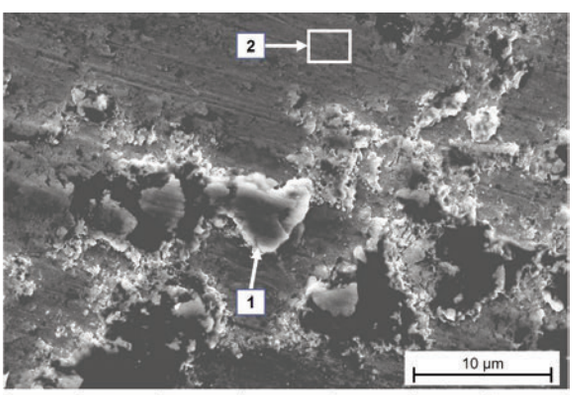

Point	Fe (wt%)	C (wt%)	Mn (wt%)	Mo (wt%)	Si (wt%)	O (wt%)
1	59.9	5.3	12.9	0.6	0.4	20.9
2	78.5	3.8	16.4	0.8	0.5	-

Figure 12. *Detailed SEM micrograph (SE mode) of worn surface for solution annealed 1.0C-17Mn alloy under 15 N*

Fig. 11 shows the SEM micrographs of worn surface of the experimental 1.0C-17Mn alloy after wear test under applied loads of 2.5 N, 5 N, 10 N and 15 N. It was observed that increased load caused an increase in the deformation on the sliding surfaces. For loads of 2.5 N, 5 N and 10 N, the main wear mechanisms were cutting furrows and pits. Increasing the load up to 10N, the amount of cutting furrows and pits increased due to the repeated plastic deformation. Since the toughness of the alloy was high and the impact load was low, chips were not easy to form and only cutting furrows and pits occurred. Fig. 11d shows that increased load from 10 N to 15 N reduced the amount of cutting furrows and pits, and changed the wear mechanism to micro-cut marks which indicated that the plastic deformation severely accelerated. The higher deformation of friction surfaces occurred

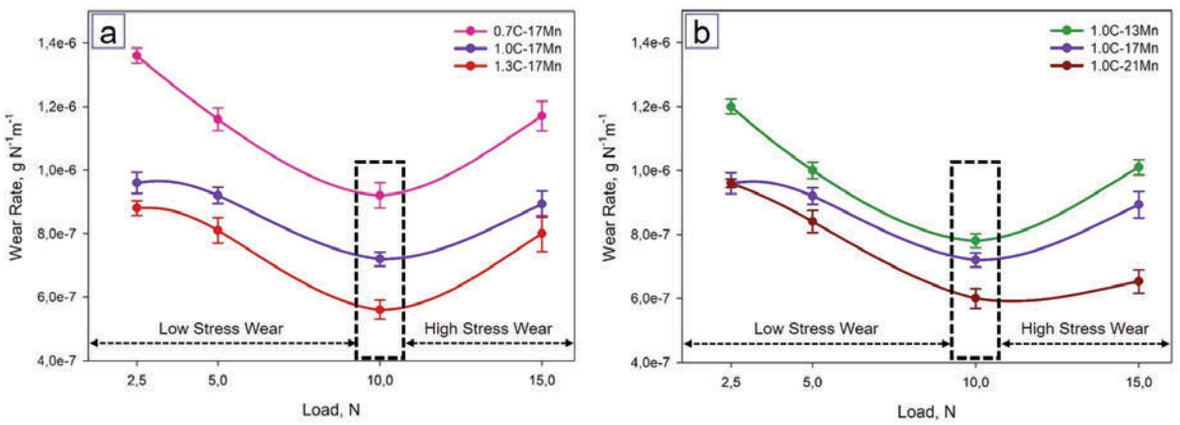

Figure 13. *Wear rate of solution annealed alloys in the various loads as a function of (a) Carbon and (b) Manganese content*

because of the presence of interface metal oxide particles (wear debris) of deformed materials as shown in Fig. 12. These particles were free to roll in the interface between alumina ball and base metal during the test and rolled particles pressed in the interface led to severe plastic deformation on the worn surface as it was reported in previous study ref. [31] and [39].

Fig. 13 illustrates wear rates of the experimental alloys after 500m sliding under varying loads at 0.2 $m.s^{-1}$ sliding speed. The trends for all the samples were roughly the same and there was a general decrease in the wear rate with increased carbon (Fig. 13a) and manganese (Fig. 13b) content. Up to 10N, the wear rate decreased. However, when the load was increased to 15N, the wear rate of all alloys sharply increased due to wear debris caused by repeated plastic deformation. On the other hand, the severity of the wear process could be placed in two categories: first is low-stress wear which involves the passage of the abrasive material once over the surface of the sample, and second is high-stress wear which involves cutting marks between two surfaces [40]. In this case, it can be concluded the wear test was a high-stress condition when the applied load was higher than 10N, while for loads lower than 10N the test can be considered to be low stress wear.

At low-stress conditions, slight work hardening of the worn surface occurred because the amount of plastic strain of the surface was very low. Therefore, the initial surface hardness and the yield strength of the alloys controlled the wear rate and the frictional wear occurred more often than shearing wear [41]. Since carbon and manganese increased the hardness and yield strength of alloys, they reduced the wear rate. Hence, the 1.3C-17Mn alloy showed better wear resistance at the low-stress wear condition due to its higher surface hardness and yield strength caused by the existence of hard carbides dispersed within the austenite matrix, respectively, 437.1±7.1 MPa and 208±2 HB.

At the high-stress wear condition, severe plastic deformation of the worn surface occurred because the scratching of the worn surface was too high that the wear debris was removed. Although the higher results in terms of toughness, tensile strength, and elongation were obtained in 1.0C-17Mn alloy, 1.0C-21Mn alloy showed superior wear resistance, especially under high-stress wear of a 15N normal load, which was about 21% better than 1.0C-17Mn alloy. This was due to an increase in austenite stability resulted from increased manganese content. Moreover, the wear rate of 1.3C-17Mn sharply increased in contrast with that 1.0C-21Mn alloy when the applied load was raised to 15N, the wear rate of 1.3C-17Mn was 23 % higher than that of 1.0C-21Mn. Therefore, 1C-21Mn alloy could be applied to relatively high-stress wear conditions, while the 1.3C-17Mn alloy could be only used under low-stress wear conditions due to their insufficient impact toughness.

4. Conclusions

The microstructure of the as-cast alloys consisted of an austenite matrix with two main $(Fe,Mn)_3C$ and MoC complex carbides along the grain boundaries. The carbon and manganese in the as-cast state increased the carbide content. They also increased the grain size of the as-cast alloys due to extending the freezing range of the alloys. In the samples with the fixed manganese content of 17 wt%, increasing the carbon content transformed the tiny grain boundary carbides to the lamellar ones. The net effect of increasing carbon content was improved yield strength and hardness of the alloys. The as-cast states showed brittle failure during tensile tests with limited plastic deformation and low ductility.

The solution annealing fully dissolved the carbides of the alloy with lower carbon content (1

wt%) and yielded a fully austenitic microstructure; however, it did not fully dissolve the grain boundary carbides of alloys with carbon content up to 1.3 wt%. Higher solution temperature may dissolve the carbides; however, it will increase the grain size and may deteriorate the mechanical properties. The designed solution annealing improved the hardness of all the as-cast alloys, except for the 1.3C-17Mn and 1.0C-21Mn. The decrease in hardness was dependent on the morphology and distribution of the carbides in the as-cast and solution annealed states. The solution annealing increased the ductility of the as-cast alloys by the dissolution of the brittle carbides in the austenite matrix. However, the highest tensile strength and ductility was observed in 1.0C-17Mn alloy.

The main deformation mechanism was twinning which is easily formed in 1.0C-17Mn alloy, while it was absent in 1.3C-17Mn alloy. The solution annealing significantly increased the toughness of the as-cast alloys with the highest improvement at almost ~930 % increase in the 1.0C-17Mn. The less pronounced effect in the alloys with higher carbon content was due to incomplete dissolution of the carbides.

Increasing carbon and manganese contents resulted in a decrease in wear rate. The 1.3C-17Mn alloy showed better wear resistance at the low-stress wear condition due to its higher surface hardness and yield strength. However, under the high-stress condition, the 1.0C-21Mn alloy showed superior wear resistance which is about 27 % and 18 % better than 1.0C-17Mn and 1.3C-17Mn steels, respectively. Therefore, 1C-21Mn alloy could be applied in relatively high impact abrasive conditions while the 1.3C-17Mn alloy could be only used under low impact abrasive conditions due to their insufficient impact toughness.

Acknowledgments

The authors are grateful to the Sakarya University and Silvan Sanayi A.Ş. for the support of this research and for the provision of laboratory facilities.

References

[1] H. Maouche, A. Hadji, K. Bouhamla, Metall. Min. Ind., 3 (2016) 75-82.

[2] S. W. Bhero, B. Nyembe, K. Lentsoana, ICMMME, 15-16 April, Johannesburg, South Africa, 2014, p.17-19.

[3] B. J. Sutton, Masters Thesis, Columbus, The Ohio State University, 2013.

[4] C. S. Mahlami, X. Pan, Proc. 71st WFC, 19-21 May, Bilbao, Spain, 2014, p.420-428

[5] J. O. Agunsoye, S. I. Talabi, O. Bello, Adv. Produc. Eng. Manag., 10 (2) (2015) 97-107.

[6] B. Bal, Int. J. Steel Struct., 18 (1) (2018) 13-23.

[7] N. D. Nam, L.T. Chieu, N.M Truc, P. M. Khanh, Int. J. Sci. Eng. Res., 7 (4) (2016) 1527-1530.

[8] A. K. Srivastava, K. Das, J. Mater. Sci., 43 (2008) 5654–5658.

[9] S. H. M. Anijdan, M. Sabzi, J. Mater. Eng. Perform, 27 (10) (2018) 5246-5253.

[10] M. Azadi, A. M. Pazuki, M. J. Olya, Metallogr. Microstruct. Anal., 7 (2018) 618-626.

[11] F. Haakonsen, Ph.D. Thesis, Trondheim, Norwegian University of Science and Technology, 2009.

[12] Y. S. Ham, J. K. Kim, S. Y. Kwak, J. K. Choi, W.Y. Yoon, China Foundry, 7 (2) (2010) 178-182.

[13] F. Nurjaman, F. Bahfie, W. Astuti, A. Shofi, 2nd ISFAP, 3-5 October, Jakarta, Indonesia, 2017, p1-7.

[14] S. A. Balogun, D. E. Esezobor, J.O. Agunsoye, J. Min. Mater. Char. Eng., 7 (3) (2008) 277-289.

[15] H. Hosseini, M. Limooei, World Appl. Sci. J., 15 (10) (2011) 1421-1424.

[16] I. El-Mahallawi, R. Abdel-Karim, A. Naguib, Mater. Sci. Tech-Lond., 17 (2001) 1385-1390.

[17] M. K. Pham, D. N. Nguyen, A. T. Hoang, Int. J. Mechanical & Mechatronics Eng., 18 (2) (2018) 141-147.

[18] J. L. Cao, A. M. Zhao, J. X. Liu, J. G. He, R. Ding, J. Iron Steel Res. Int., 21 (6) (2014) 600-605.

[19] G. Tęcza, A. G. Klempka, Arch. Foundry Eng., 16 (4) (2016) 163-168.

[20] J. O. Agunsoye, T. S. Isaac, A. A. Abiona, J. Miner. Mater. Char. Eng., 1 (2013) 24-28.

[21] F. Maratray, International Manganese Institute, Paris, France, 1995.

[22] X. Yuan, L. Chen, Y. Zhao, H. Di, F. Zhu, J. Mater. Process Tech., 217 (2015) 278-285.

[23] L. Dingshan, L. Zhongyi, L. Wei, China Foundry, 11 (3) (2014) 173-178.

[24] S. A. Torabi, K. Amini, M. Naseri, Int. J. Adv. Design Manuf. Tech., 10 (1) (2017) 75-83.

[25] L. G. Korshunov, I. I. Kositsina, V. V. Sagaradze, N. L. Chernenko, Phys. Met. Metallogr., 112 (1) (2011) 90-100

[26] M. Mohammadnezhad, V. Javaheri, M. Naseri, The Second International and the Seventh Joint Conference of Iranian Metallurgical Engineering and Iranian Foundaryman Scintific Societies, 30-31 October, Semnan, Iran, 2013, 12816

[27] S. Kuyucak, R. Zavadil, AFS Trans.108, Paper No.00-126, 2000.

[28] D. K Subramanyam, A. E. Swansiger, H. S. Avery, ASM International, 1991, p.240.

[29] S. Kuyucak, R. Zavadil, AFS Trans.109, Paper No. 01-117, 2001.

[30] B. N. Venturelli, E. Albertin, C. R. F. Azevedo, Mater. Res., 21 (5) (2018) 1-8.

[31] U. Lee, S. S. Sohn, S. Hong, B. C. Suh, S. K. Kim, B. J. Lee, N. J. Kim, S. Lee, Metall. Mater. Trans. A, 45 (A) (2014) 5419-5430.

[32] D. Canadinc, H. Sehitoglu, H. J. Maier, D. Niklasch Y.I. Chumlyakov, Int. J. Solids Struct., 44 (2007) 34–50

[33] N. K. Tewary, S. K. Ghosh S. Chatterjee, J. Mech., 233 (3) (2017) 763-771.

[34] C. Okechukwu, O. A. Dahunsi, P. K. Oke, I. O. Oladele and M. Dauda, Int. J. Eng. Tech., 3 (2) (2017)

83-90.

[35] M. Sabzi, S. M. Dezfuli, J. Manuf. Process, 34 (2018) 313-328.

[36] J. O. Olawale, S. A. Ibitoye, M. D. Shittu, Mater. Res., 16 (6) (2013) 1274-1281.

[37] J. O. Agunsoye, T. S. Isaac, A. A. Abiona, J. Miner. Mater. Char. Eng., 1 (2013) 24-28.

[38] X. J. Wang, X. J. Sun, C. Song, H. Chen, S. Tong, W. Han and F. Pan, Acta Metall. Sin. Engl., 32 (16) (2019) 746-754.

[39] P. C. Astudillo, A. F. Soriano, G. M. B. Osorio, H. S. Sthepa, J. Ramos, J. F. Duran, G. A. P. Alcazar, Hyperfine Interact, 238 (56) (2017) 1-12.

[40] D. R. Marsano, Masters Thesis, Golden, Colorado School of Mines, 2000.

[41] M. M. Atabaki, S. JafariIv, H. Abdollah-pour, J. Iron Steel Res. Int., 19 (4) (2012) 43-50.

UTICAJ SADRŽAJA UGLJENIKA I MANGANA NA MIKROSTRUKTURU I MEHANIČKE OSOBINE AUSTENITNOG ČELIKA SA VISOKIM SADRŽAJEM MANGANA

U. Gürol [a*], S. Can Kurnaz [a]

[a] Univerzitet u Sakarji, Inženjerski fakultet, Odsek za metalurško inženjerstvo i inženjerstvo materijala, Sakarja, Turska

Apstrakt

U ovom radu su ispitivani uticaji ugljenika i mangana na mikrostrukturu i mehaničke osobine austenitnog čelika sa visokim sadržajem mangana. Povećan sadržaj ugljenika i mangana povećao je veličinu zrna i količinu karbida u izlivenom stanju. Rastvorno žarenje je u potpunosti rastopilo karbide u legurama sa nižim sadržajem ugljenika (1wt%) i rezultiralo homogenom austenitnom mikrostrukturom. Čvrstoća na istezanje, kritična čvrstoća, Šarpi, i elongacija povećani su kombinacijom ugljenika i mangana. Optimalni rezultatisu dobijeni kod rastvorno žarene 1.0C-17Mn legure, pojedinačno 415.0±4.1MPa 865.6±1.5 MPa, 65.2±0.8% i 258±3 J. Testiranje na habanje je urađeno sa opterećenjima od 5N, 10N i 15N na ‚kugla-na-disku' mašini za ispitivanje habanja pri konstantnoj brzini od 0.2 ms-1 za dužinu klizanja od 500m, i pokazalo se da 1C-21Mn legura može da se primeni za uslove habanja sa relativno visokim naprezanjem dok 1.3C-17Mn legura može da se primeni za uslove habanja sa niskim naprezanjem.

Ključne reči: *Hadfield čelik; Karakterizacija mikrostrukture; Otpornost na istezanje; Žilavost po Šarpiju; Otpornost na habanje*